Soft Matter

PAPER

View Article Online
View Journal | View Issue

Cite this: *Soft Matter*, 2019, **15**, 6547

Can one determine the density of an individual synthetic macromolecule?†‡

Daniel Messmer, *[a] Antoni Sánchez-Ferrer, [b] Sebastian Tacke,§[c] Hao Yu, ¶[a] Harald Nüsse,[d] Jürgen Klingauf,[d] Roger Wepf, ‖[d] Martin Kröger, [a] Avraham Halperin,**[e] Raffaele Mezzenga *[b] and A. Dieter Schlüter *[a]

Received 19th June 2019,
Accepted 16th July 2019

DOI: 10.1039/c9sm01220f

rsc.li/soft-matter-journal

Dendronized polymers (DPs) are large and compact main-chain linear polymers with a cylindrical shape and cross-sectional diameters of up to ~15 nm. They are therefore considered molecular objects, and it was of interest whether given their experimentally accessible, well-defined dimensions, the density of individual DPs could be determined. We present measurements on individual, deposited DP chains, providing molecular dimensions from scanning and transmission electron microscopy and mass-per-length values from quantitative scanning transmission electron microscopy. These results are compared with density values obtained from small-angle X-ray scattering on annealed bulk specimen and with classical envelope density measurements, obtained using hydrostatic weighing or a density gradient column. The samples investigated comprise a series of DPs with side groups of dendritic generations g = 1–8. The key findings are a very large spread of the density values over all samples and methods, and a consistent increase of densities with g over all methods. While this work highlights the advantages and limitations of the applied methods, it does not provide a conclusive answer to the question of which method(s) to use for the determination of densities of individual molecular objects. We are nevertheless confident that these first attempts to answer this challenging question will stimulate more research into this important aspect of polymer and soft matter science.

Introduction

The bulk volumetric mass densities ρ of organic polymers generally lie between $\rho \approx 0.84$ g cm^{-3} for poly(4-methylpent-1-ene) and $\rho \approx 2.3$ g cm^{-3} for poly(tetrafluoroethylene).[1] The high mechanical strength of many polymers at their usually low density is one of the main driving forces for the application of polymers *e.g.* in the automotive industry. The bulk density depends on a complex interplay between composition, structure, and molecular packing. While various properties of individual polymer chains have been studied, including tensile strength[2–5] and chain flexibility,[6] density has to the best of our knowledge not been investigated on a molecular scale. In no small part, this is due to the difficulty in determining a molecule's volume. On the nanoscale, even the definition of molecular volume is not exactly straightforward, and researchers rely on a variety of quantities (*e.g.* hydrodynamic, van der Waals, solvent accessible, or Voronoi volumes). It is easier to define and determine the

[a] *Department of Materials, ETH Zürich, Polymer Chemistry & Polymer Physics, Vladimir-Prelog-Weg 5, 8093 Zürich, Switzerland. E-mail: daniel.messmer@mat.ethz.ch, dieter.schluter@mat.ethz.ch*

[b] *Department of Health Sciences and Technology, ETH Zürich, Laboratory of Food and Soft Materials, Schmelzbergstrasse 9, 8092 Zürich, Switzerland. E-mail: raffaele.mezzenga@hest.ethz.ch*

[c] *Scientific Center for Optical and Electron Microscopy, ETH Zürich, Otto-Stern-Weg 3, 8093 Zürich, Switzerland*

[d] *Institute of Medial Physics and Biophysics, Westfälische Wilhelms-Universität Münster, Robert-Koch-Strasse 31, 48149 Münster, Germany*

[e] *Laboratoire de Spectrometrie Physique, CNRS University Joseph Fourier, BP 87, 38402 Saint Martin d'Hères cedex, France*

† This work is dedicated to the memory of Avraham (Avi) Halperin, who was a long-term collaborator of many of the authors. We feel grateful for having had the chance to interact with Avi, a man of great insight and humor. Though he did not witness the completion of this article, he motivated much of the work presented here, and accompanied it for as long as his health permitted, until shortly before his passing. Both as scientists and as personal acquaintances, we miss Avi greatly, and we would like to express our condolences to his family.

‡ Electronic supplementary information (ESI) available: Details on experimental procedures, evaluation of the results, LabView code used in the evaluation of qSTEM, extensive discussion of possible errors for density determination. See DOI: 10.1039/c9sm01220f

§ Current address: MPI for Molecular Physiology, Structural Biochemistry, Otto-Hahn-Strasse 1, 44227 Dortmund, Germany.

¶ Current address: Laboratory of Packaging Engineering, School of Printing and Packaging, Wuhan University, 430000 Wuhan, People's Republic of China.

‖ Current address: Center for Microscopy and Microanalysis, University of Queensland, St. Lucia, Queensland 4072, Australia.

** A. Halperin unfortunately passed away during the preparation of this publication.

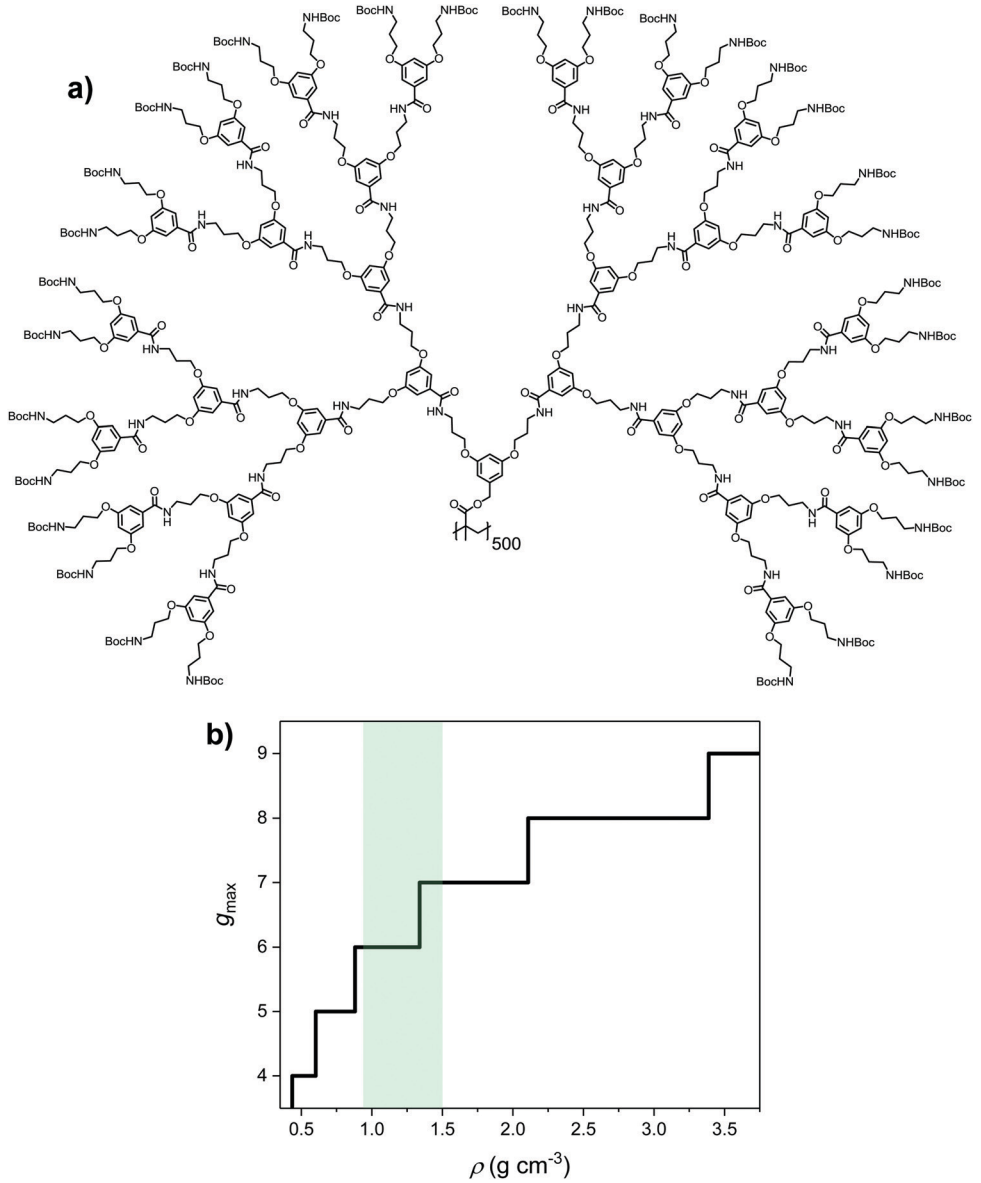

Fig. 1 (a) Chemical structure of one representative (PG5) of the series of DPs investigated in this publication. Generally, dendronized polymers are linear polymers with dendritic (*i.e.* repeatedly and regularly branched) side groups attached to each repeating unit. (b) Estimate of the maximum theoretically accessible dendritic (*i.e.* defect-free) side-chain generation g_{max} as a function of ρ. Using the previously estimated density range of ρ = 0.9–1.5 g cm^{-3} marked in green, one obtains $g_{max} \approx 6$–7.[17]

volume – and hence the density – when molecules with extended dimensions are considered, rather than classical linear polymers. Dendronized polymers (DPs, Fig. 1a) are one example of such "molecular objects".[7,8] Other examples of macromolecules which may in some cases be considered molecular objects include hypergraft[9,10] and bottle-brush copolymers,[11] dendrimers,[12] and hyperbranched polymers.[13,14] Given the achievable sizes of such molecular objects – DPs may reach up to ~15 nm in diameter and several μm in length – the volume and thus the density of an individual macromolecule may in principle be measured.

Determining the density of molecular objects is of particular interest for the most well-defined structures among those mentioned, *i.e.* dendrimers and DPs, especially as a function of the dendritic generation number *g*. *g* corresponds to the number of branching points within one arm of a dendritic (*i.e.*, repeatedly and regularly branched) structure. An increase in *g* goes along with a substantial increase in molar mass that might cause variations in packing geometry, backfolding tendencies *etc.*, which in turn potentially affect the overall density of the molecular object. An adjacent point of interest for dendritic structures is the fact that ρ determines the location of the maximum dendritic generation number g_{max}, up to which a dendritic macromolecule can theoretically be obtained without defects.[15,16] This synthetic limit exists for any dendritic structure, due to the fact that the extension of a dendron grows linearly with *g* while its molar mass grows exponentially.

There is therefore always a value of g – dependent on ρ, see Fig. 1b – above which the mass of a structurally perfect dendron cannot be accommodated within the maximum volume defined by the molecular structure. For the type of DP that this publication is concerned with (see Fig. 1a), this value has been estimated to lie in the range $6 \leq g_{max} \leq 7$.[17] The largest factor of uncertainty in this estimate is the volumetric mass density ρ, which has previously been determined only for DPs of $g < g_{max}$: a combination of scanning and transmission electron microscopy (SEM and TEM) imaging of adsorbed DPs permitted the calculation of densities in the range $\rho_{SEM/TEM} \approx 1.35$–$1.45$ g cm^{-3} for the DPs of g = 1–5 (PG1–PG5).[17] Similarly, small-angle X-ray scattering (SAXS) measurements in the bulk resulted in a rough estimate of the density of a g = 4 DP (PG4) of ρ = 1.46 g cm^{-3}.[18] MD simulations of short DPs ($P_n \leq 100$) in vacuum suggested a modest increase in the average density with g, from ρ = 0.97 g cm^{-3} for g = 1 to ρ = 1.1 g cm^{-3} for g = 6,[19,20] closely matching values obtained for PAMAM dendrimers by Goddard *et al.*[21]

In this publication, we report density measurements on a series of DPs of g = 1–8, *i.e.* in part above the estimated g_{max}. Classical envelope density determination using hydrostatic weighing and a density gradient column on compact DP samples supplement the derivation of density values from different molecular-scale measurements: packing parameters of self-assembled DP domains in compact samples were obtained by SAXS, individual molecule dimensions were measured by a combination of SEM and TEM, and mass maps were obtained by quantitative scanning transmission electron microscopy (qSTEM). We discuss the respective density values (ρ_{bulk}, ρ_{SAXS}, $\rho_{SEM/TEM}$, ρ_{qSTEM}) as well as strengths and weaknesses of the methods applied, with a particular focus on potential sources of error and the assumptions or models necessary to derive density values. As the determination of density in polydisperse, individual molecules is a hitherto unexplored field, the focus of this study lies on the evaluation of the applied methods, and on suggesting alternative methods which may alleviate the observed issues.

Experimental

Polymers

The DPs discussed in this publication are for the most part the members of a series A, containing PGg ranging from g = 1 to g = 8 with a uniform main-chain length of $P_n \approx 500$. They were prepared using a graft-from protocol as described previously.[22,23] Series A is not strictly homologous, in that the DPs of g = 6 and g = 8 (PG6 and PG8) were prepared from the corresponding ($g - 2$) precursors, *i.e.* PG4 and PG6, respectively. This protocol involved the use of a bulky g = 2 dendronization agent,[24] and therefore the defect frequency in the $g > 5$ DPs was high compared to all preceding dendronization steps. Synthetic advances enabled the preparation of a strictly homologous series of DPs (series B).[25] The $g > 4$ members of series B are also discussed briefly, though density determination is limited to ρ_{bulk} and ρ_{SAXS} (see ESI‡ Section 3). The quantification of defects in both series was achieved by labelling of residual, unreacted amines as discussed elsewhere.[25–28] By this measure, PG6 in series A is missing ~10% (corresponding to *ca.* 1 MDa for a 500 mer), whereas PG6 in series B lacks merely 1.3% (≈140 kDa) of the theoretically achievable mass. The defect quantification afforded the mass-per-length (MPL) values M_{label} used in the calculation of ρ_{SAXS} and $\rho_{SEM/TEM}$ (see ESI,‡ Tables S1 and S2).

Compact cylindrical pills of the DPs (∅ 4 mm, 1–4 mm thick) were prepared by vacuum hot-pressing of the loose, freeze-dried polymer powders (see ESI,‡ subsection 1.4 for details). These polymer pills (likely still containing trace residual solvent from the freeze-drying process) were annealed in an in-house built high vacuum oven ($p \approx 5 \times 10^{-9}$ mbar) at 120 °C ($T > T_g$)[29] for 7 d. These annealed pills were employed for density gradient column and SAXS measurements.

Measurement of ρ_{bulk} by hydrostatic weighing

The density of annealed DP pills was determined by the Archimedean method (hydrostatic weighing) using an analytical balance (Mettler Toledo AE 163) and a fitting density determination kit (Mettler Toledo, catalogue number ME-40290), using hexane as the displaced fluid.

Measurement of ρ_{bulk} using a density gradient column

Density gradients were established in a simple in-house built density gradient column setup (see ESI,‡ Fig. S4) using aqueous solutions of sodium bromide (Acros Organics) as the fluid medium (working range approximately 1.0–1.5 g cm^{-3}). Samples (annealed DP pills) and calibration standards (hollow glass spheres, H&D Fitzgerald Ltd) were set into the bottom of the column. The column was filled from the bottom by slow aspiration of the gradient mixture (initially deionized water, containing a steadily increasing concentration of sodium bromide, see ESI,‡ subsection 2.2 for details). The resulting density gradient column was left to stand undisturbed overnight for equilibration before the positions of calibration standards and DP samples were determined.

SAXS

Simultaneous SAXS and WAXS measurements of annealed DP pills were conducted either on an AXS Micro (Bruker) equipped with a microfocused beam (50 W, 50 kV, 1 mA, $\lambda_{CuK\alpha}$ = 0.15418 nm) and a Dectris 2D 100 K X-ray detector (Pilatus, 83.8 cm × 33.5 cm, 172 μm resolution; an effective scattering vector range of 0.1 nm^{-1} < q < 25 nm^{-1} was obtained) or on a MicroMax-002$^+$ (Rigaku) equipped with a microfocused beam (40 W, 45 kV, 0.88 mA, $\lambda_{CuK\alpha}$ = 0.15418 nm) collimated by three pinhole collimators (0.4, 0.3, and 0.8 mm), a Triton-200 gas-filled detector (20 cm diameter, 200 μm resolution) and a two-dimensional BAS-MS 2025 imaging plate system (Fujifilm, 15.2 × 15.2 cm^2, 50 μm resolution; an effective scattering vector range of 0.05 nm^{-1} < q < 25 nm^{-1} was obtained). Experiments were conducted at RT and the DP pills were affixed in the sample holder with a piece of adhesive tape, which was measured without a sample for background subtraction.

SEM & TEM

Samples for SEM were prepared by drop-casting solutions of DPs (1–5 mg L^{-1} in methylene chloride) onto freshly cleaved mica. The samples were air-dried, then transferred to a vacuum

Table 1 Density values obtained as a function of dendritic generation g (compare Fig. 4)

	PG1	PG2	PG3	PG4	PG5	PG6	PG7	PG8
ρ_{bulk} [g cm^{-3}] (hydrostatic weighing)[a]	1.16 ± 0.02	1.18 ± 0.02	1.19 ± 0.02	1.21 ± 0.01	1.20 ± 0.02	1.23 ± 0.01	1.22 ± 0.03	1.24 ± 0.04
ρ_{bulk} [g cm^{-3}] (density gradient column)[ab]	1.153 ± 0.001	1.183 ± 0.001	1.194 ± 0.002	1.20 ± 0.01	1.199 ± 0.002	1.232 ± 0.008	1.205 ± 0.001	1.215 ± 0.001
ρ_{SAXS} [g cm^{-3}] (rhombohedral columnar)	—[c]	—[c]	0.90 ± 0.13	0.97 ± 0.08	1.00 ± 0.04	1.29 ± 0.09	2.97 ± 0.13	2.9 ± 0.3
$\rho_{SEM/TEM}$ [g cm^{-3}] (cut-circle cross-section)	—[c]	1.3 ± 0.4[d]	1.3 ± 0.3[d]	1.4 ± 0.2[d]	1. 3 ± 0.1[d]	2.2 ± 0.3	2.4 ± 0.4	2.1 ± 0.6
ρ_{qSTEM} [g cm^{-3}] (cut-circle cross-section)	—[c]	—[c]	—[c]	—[c]	1.34 ± 0.04	1.46 ± 0.05	1.32 ± 0.07	1.82 ± 0.11

[a] Average values calculated from the densities of individual DP samples as shown in Fig. 3a. [b] Errors are standard deviations of the average; errors of individual samples from density gradient column measurements are negligible (<±0.001 g cm^{-3}). [c] Value not determined. [d] See ref. 17.

chamber for metal coating (Bal-Tec BAF060). A uniform tungsten coating of *ca.* 1 nm was applied by rotary shadowing at an elevation angle of 45°. SEM images were recorded on a LEO 1530 cryo-FE-SEM (Zeiss) simultaneously in the SE and BSE modes using acceleration voltages in the range of 2–10 kV.

Specimen for TEM were likewise prepared by drop-casting methylene chloride solutions (containing 1–5 mg L^{-1} DP) onto freshly cleaved mica. The samples were air-dried, then transferred into a metal coating device (Bal-Tec BAF060). The surface was unidirectionally shadowed with tungsten (6 nm, applied at an elevation angle of 7°). Then, an additional layer of carbon (8 nm, 90°) was applied. The samples were removed from the chamber, the carbon replicas were floated off the surfaces and deposited onto copper TEM grids (400 mesh, Plano GmbH) and the samples were dried in air. Images were recorded on a CM12 TEM (Phillips/FEI, 120 kV acceleration voltage).

qSTEM

Samples were prepared by placing a droplet (~5 μL) of a DP solution (~2 mg L^{-1} in methylene chloride) onto a TEM grid carrying a thin layer of amorphous carbon (1–2 nm) atop a lacey carbon film. Excess liquid was blotted off, the grid was immediately plunged into liquid nitrogen and then transferred into a vacuum chamber for freeze-drying. To avoid contamination, the grids were thereafter transferred using a high vacuum cryo shuttle.[30] The samples were briefly surveyed for quality by SEM imaging (Merlin FE-SEM, Zeiss) and then transferred into an STEM (Hitachi S5000 SEM equipped with an ADF-detector, operating in STEM mode) operating at 30 kV in low-dose mode (300–500 e nm^{-2}); the nominal pixel size was 0.699 nm. The data analysis is describe in the ESI‡ (subsection 2.5).

Results

The results presented here correspond to density measurements conducted on the DPs of series A (ranging from g = 1–8) for which all methods were applied when possible (see Table 1).†† Additional results (ρ_{bulk} and ρ_{SAXS}) for the structurally less deficient DPs of series B (members of g = 5–8) are only briefly discussed in the main text; details can be found in the ESI‡ (Section 3).

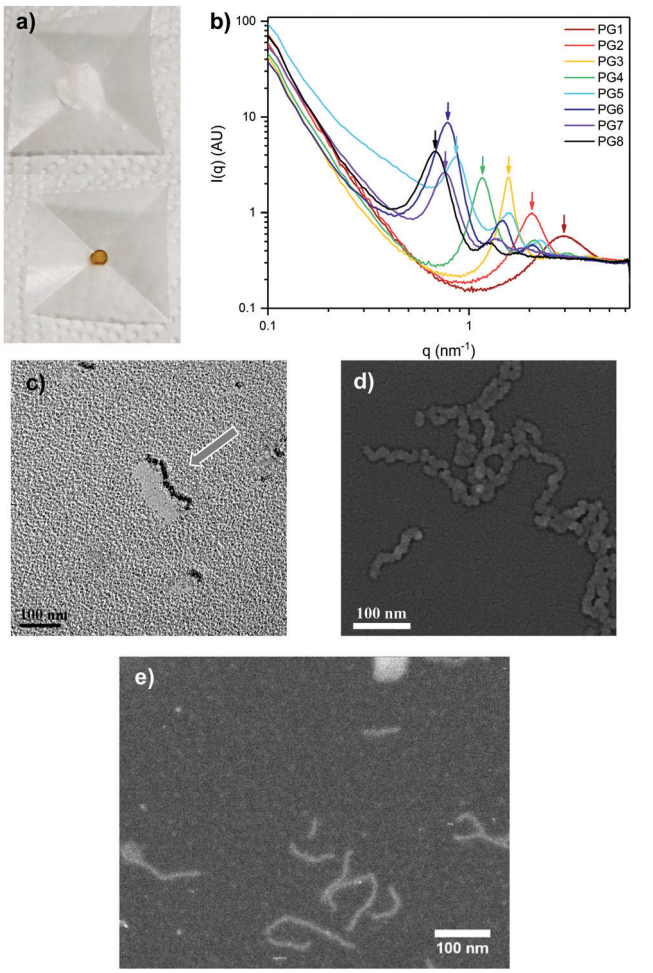

Fig. 2 (a) Comparison of freeze-dried PG4 powder (top) and a compact, annealed pill of the same polymer (bottom); both samples weigh *ca.* 18 mg; (b) SAXS curves (PG1–PG8) used for the estimate of ρ_{SAXS}; (c) TEM image (carbon replica of a unidirectionally W-shadowed specimen; arrow indicates the direction of sputtering) and (d) SEM image (rotary W-shadowed) of PG5 on mica used in the determination of $\rho_{SEM/TEM}$; (e) low-dose STEM image of PG5 deposited on a thin film of amorphous carbon used in the derivation of ρ_{qSTEM}.

†† The results are presented in an order intended to facilitate the discussion of the various methods and results. The measurements of $\rho_{SEM/TEM}$ predate the others, extending previously published results[17] to g = 8. The startlingly high density values observed in these measurements prompted the application of the other methods discussed in this paper.

Measurement of bulk envelope densities (ρ_{bulk})

The envelope density values ρ_{bulk} obtained for several samples per generation (Fig. 2a) are shown in Fig. 3a. The values obtained by hydrostatic weighing closely match those determined by density gradient column, though the latter are more precise and the scatter between individual DP pill densities is lower for the same samples. The lack of precision in hydrostatic weighing is largely owed to the small sample size (10–30 mg).

Bulk density values are influenced by the proportions of amorphous *vs.* self-assembled domains, packing geometry, and the DP chains' capacity for deformation or interpenetration. ρ_{bulk} does therefore not permit a reliable derivation of the aimed-for individual molecule density values. However, particularly the density gradient column measurements provide precise density values without requiring external assumptions. Therefore, ρ_{bulk} is useful as a benchmark value: it sets a hard lower limit for individual molecule density and helps in evaluating the results from other methods. The data in Fig. 3a suggest a modest overall increase in ρ_{bulk} with growing g, from ρ_{bulk} = 1.15 g cm^{-3} for PG1 to $\rho_{bulk} \approx$ 1.22 g cm^{-3} for PG8 (Table 1). The modest variations in ρ_{bulk} between individual samples of the same material as determined by the more precise density gradient column method (maximum $\pm$ 0.01 g cm^{-3}) might stem from variations in DP packing, which unfortunately was not readily quantifiable *e.g.* by DSC, as the DPs decompose prior to melting.[23]

Determination of individual-molecule density based on packing geometry from SAXS (ρ_{SAXS})

The dendronized polymers of g = 1–8 discussed here are generally brittle solids at room temperature, with glass transition temperatures T_g in the range of 40–70 °C.[29] For convenience of handling, they were usually stored as freeze-dried powders rather than as bulk solids.[22,23,25] Already in the crude, freeze-dried state, preliminary investigations by SAXS indicated some self-assembly into fibre bundles for the DPs of $3 \leq g \leq 6$ (see ESI,‡ Fig. S21, also compare ref. 18). By hot-pressing and vacuum annealing of the DP samples at $T > T_g$ (Fig. 2a), the number of Bragg peaks increased, and the scattering curves of all samples of $g > 2$ contained three or more reflexes (Fig. 2b, see ESI,‡ Fig. S6, for individual SAXS curves and fits). As expected for molecular objects of increasing diameter, the primary scattering peak continuously shifted to lower q values with increasing g. For all DP samples, simultaneously conducted WAXS experiments revealed one broad, unstructured signal at $q \approx$ 13.5 nm^{-1} for DPs of all g (see ESI,‡ Fig. S22). This indicates that the DP side chains are essentially amorphous, and no significant differences in intramolecular packing are apparent between DPs of different g.

For the $g > 2$ DPs, the SAXS results permit the determination of intermolecular packing parameters. We refrained from including results for PG1 and PG2 in Fig. 2b and Table 1, as these DPs are essentially amorphous. In combination with molar mass values obtained from the defect quantification of the DPs (M_{exp}, see ESI,‡ Tables S1 and S2) and the length of the repeat unit L_{RU}, these parameters provide an estimate of individual-chain density within the ordered domains of the bulk samples (see ESI,‡ subsection 2.3). The density depends heavily on the assumed packing geometry. Rhombohedral columnar geometry provides the best fit with the experimental data and results in the lowest values of ρ_{SAXS} (see ESI,‡ Table S3 and Fig. S5, for results corresponding to tetragonal, hexagonal and oblique columnar packings‡‡). For this best-case fit, density values for the ordered domains in the bulk solids start at $\rho_{SAXS,PG3} \approx$ 1.08 g cm^{-3}. Density then increases, steeply so after g = 5, reaching an extraordinarily high calculated maximum density value of $\rho_{SAXS,PG7} \approx$ 3 g cm^{-3} (see Table 1).

Determination of individual-molecule density based on molecular dimensions from SEM and TEM ($\rho_{SEM/TEM}$)

TEM images of carbon replicas of unidirectionally metal-shadowed DPs provide a measure of the height (h_{TEM}) of individual, adsorbed DP chains, and SEM images of rotary-shadowed DP chains provide a measure of the width (w_{SEM}) of the same adsorbed species. Given M_{label} (see ESI,‡ Table S1) and a model for the cross-section geometry, the density for an individual DP chain $\rho_{SEM/TEM}$ can be calculated. The density values shown in Fig. 3c assume cut-circular or rectangular cross-sections.[17,19] The values shown in Fig. 3c and Table 1 include those published previously for the DPs of g = 2–5 ($\rho_{SEM/TEM} \approx$ 1.35–1.45 g cm^{-3})[17] and additionally values for the more recently prepared DPs of g = 6–8.[23] Differences between these two sections of measurements are readily apparent, the latter polymers reaching density values of $\rho_{SEM/TEM}$ in the range of 2.0–2.5 g cm^{-3}. The density of PG1 could not be determined by this method, as the deposited DP provided insufficient contrast in metal-shadowed specimen.[17]

Determination of individual-molecule density based on qSTEM-based mass-per-length measurements (ρ_{qSTEM})

Quantitative STEM (qSTEM) employs a photometric approach to determine the mass of nanoscopic particles deposited on very thin substrates. The idea of deriving the mass of objects from the quantification of scattered electron intensity in transmission mode dates back to the 1960s.[31] The same approach may be employed using standard modern STEM instruments equipped with a high angle annular dark field detector, given precise instrument calibration and knowledge of the compositions of the scattering specimen. qSTEM has been employed to determine the molar masses of proteins,[32–35] though for that purpose modern mass spectrometric techniques have proved more popular.[36,37] Unlike mass spectrometric methods however,§§ qSTEM permits determination of the mass per unit length (MPL) of polydisperse, filamentous structures (dendronized polymers or *e.g.* biological filaments such as F-Actin).¶¶ MPL values M_{qSTEM}

‡‡ Thin sections of annealed DP samples were prepared in order to independently verify the packing geometry of the self-assembled domains in the annealed DP samples. Attempts to stain the specimen did however not result in sufficient differential contrast to observe self-assembled domains.

§§ Attempts to ionize even the smallest DP discussed here (PG1, $M_n \approx$ 250 kDa) using matrix-assisted laser desorption/ionization were unsuccessful, and a mass spectrometric characterization of the DPs was therefore not possible. As an added advantage, sufficiently high-resolution qSTEM data can also provide structural information on proteins and protein complexes.

¶¶ An in-depth description of modern applications of qSTEM to the biological and materials sciences by one of the authors (S. Tacke) is currently in preparation.

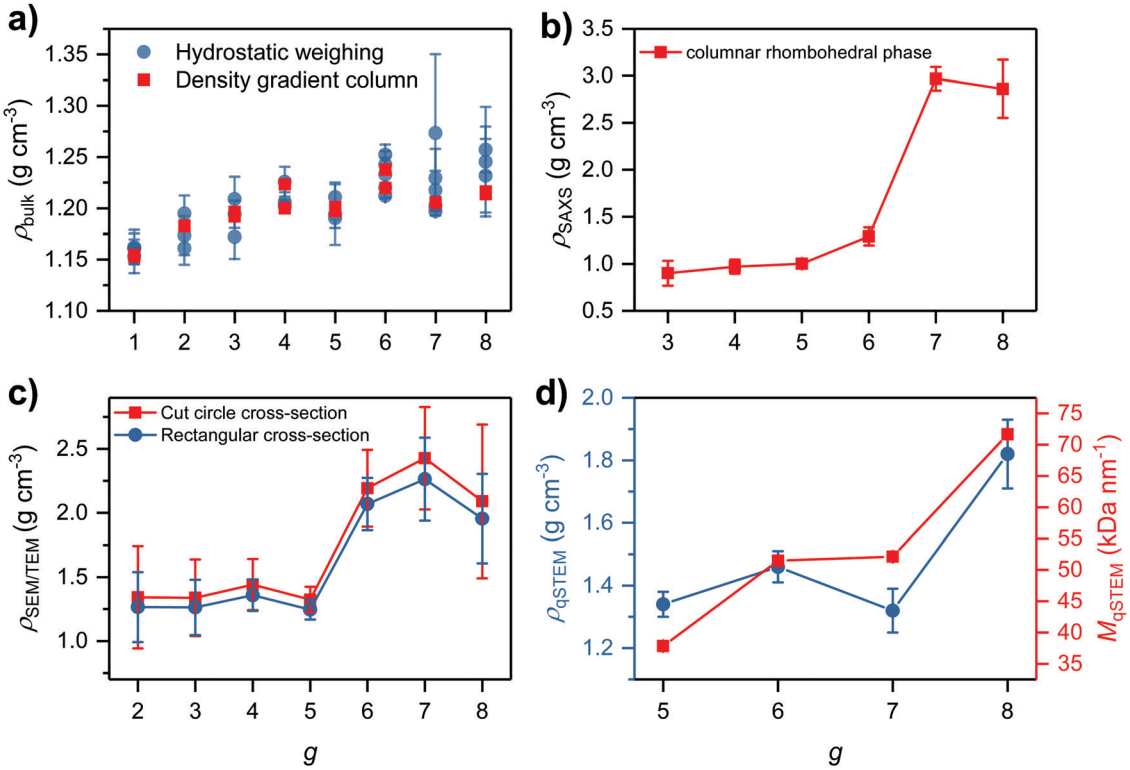

Fig. 3 Density values for DPs of g = 1–8. (a) ρ_{bulk} as determined by density gradient column and hydrostatic weighing of annealed DP pills (PG1–PG8); (b) ρ_{SAXS} as derived from SAXS measurements of annealed DP pills, assuming different packing geometries (best fit obtained with columnar rhombohedral phase); (c) $\rho_{SEM/TEM}$ obtained from the analysis of individual DP dimensions, *i.e.* the filaments' heights h_{TEM} and the widths w_{SEM}, assuming cut-circular or rectangular cross section; (d) ρ_{qSTEM} (blue, assuming cut-circular cross-section) and the mass-per-length M_{qSTEM} (red).

were obtained for DPs of g = 5–8 by averaging over the mass maps of many undisturbed DP segments (>1000 per sample) extracted from low-dose STEM images (see *e.g.* Fig. 2d). Analogous mass measurements on $g < 5$ DPs were not possible with the equipment available at the time.‖‖ The corresponding density value ρ_{qSTEM} was then calculated under the assumption of different cross-section models. Width values w_{qSTEM} were obtained directly from the qSTEM analysis, but height values necessary to determine the cross-section area of the DP chains needed to be sourced externally. Specifically, the previously discussed values h_{TEM} were employed. Assuming a cut circle cross-section model, the highest obtained density value was $\rho_{qSTEM,PG8} \approx 1.8$ g cm^{-3} (Fig. 3d).

Discussion

The density values ρ obtained using the methods described above are presented in Fig. 4 and in Table 1. ρ_{bulk} from hydrostatic weighing or density gradient column measurements provides a lower threshold for the density of the DPs for all generations, as their volume occupancy in the bulk solids cannot exceed 100%. The remaining, molecular-scale density values ρ_{SAXS}, $\rho_{SEM/TEM}$ and ρ_{qSTEM} are derived from quantities measured on individual molecules or their self-assembled

‖‖ Modern instrumentation (particularly improved detectors) might enable the investigation of DPs down to g = 3, for which MPL ≈ 10 kDa nm^{-1}.

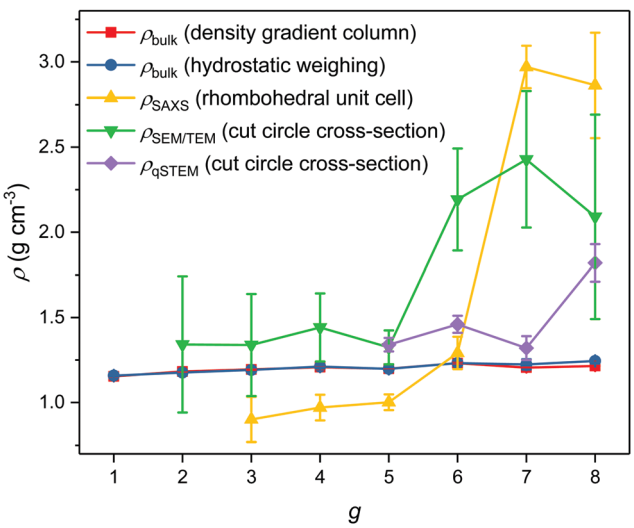

Fig. 4 Comparison of DP density values obtained by the methods employed in this publication.

structures. The resulting density data are conspicuous in three aspects: first, all methods furnish approximately similar values for $g \leq 5$, but there is substantial scatter for the higher generations. Second, extraordinarily high values of $\rho > 2.0$ g cm^{-3} are obtained for some $g > 5$ samples by SAXS and SEM/TEM, while for qSTEM, ρ does not exceed a comparatively low value of

Table 2 Key features and deficiencies of the approaches to density determination employed in this publication

Method	Information gained from measurement	Inputs for density calculation	Other potential sources of error
Hydrostatic weighing	Envelope density	—	Proportions of ordered domains; voids
Density gradient column	Envelope density	—	Proportions of ordered domains; voids
SAXS	Self-assembled domain unit cell	MPL; packing model	—
SEM/TEM	SEM: width (w_{SEM}) TEM: height (h_{TEM})	MPL; chain cross-section	Thresholding (h_{TEM} & w_{SEM}); measurements on "bumpy" objects (h_{TEM} & w_{SEM}); metal coating layer thickness (w_{SEM}); cross-section model; two different series of measurements & DPs; flattening on mica *vs.* carbon
qSTEM	Molar mass per unit length (MPL); width	Height; chain cross-section	Thresholding; height input (h_{TEM})

$\rho_{qSTEM,PG8} \approx 1.8$ g cm^{-3}. The assessment of these two observations, and therefore the evaluation of each method's reliability, is linked to the assumptions and models that were necessary to arrive at the presented density values (Table 2). A brief discussion of the sources of errors and uncertainties is presented below, and more detailed discussions may be found in the ESI‡ (Section 4). Third, though divergent in values, all methods indicate the same trend of increasing density with growing g.

Throughout the generations, the DPs have an approximately constant composition, which may be represented by the approximate empirical formula $C_{18}H_{26}N_2O_5$. This corresponds roughly to a greasy peptide such as poly(phenylalanine). For such peptides, one would expect density values generally in the range of $\rho < 1.5$ g cm^{-3}.*** As the DP side chains are compositionally and structurally quite similar to such a polypeptide, we expected overall DP densities to lie in a similar range. We therefore tentatively ascribe the high experimental density values and the substantial spread between methods observed here (Fig. 4 and Table 1) to issues with the derivation of the individual values, rather than deeming them representative of actual, very large ($>\pm0.2$ g cm^{-3}) deviations from the expected volumetric mass density. This notion is supported by wide-angle X-ray scattering (WAXS) measurements conducted in conjunction with SAXS (see ESI,‡ Fig. S22). The WAXS profiles are essentially uniform across samples of all g and suggest that the DP side chains are amorphous throughout, *i.e.* that the intramolecular packing in the dry state is not substantially affected by the increasing g.

It is notable that the two methods resulting in the highest density values – SAXS and SEM/TEM – both depend on a common external input, namely the mass per repeat unit. A thorough quantification of dendritic defects has been performed on both DP series discussed here[22,23,25,26,28] but due to the specifics of the synthesis of the $g > 5$ DPs of series A, uncertainties in MPL values remain. It is possible that the MPL values used in calculating ρ_{SAXS} and $\rho_{SEM/TEM}$ (M_{label}, see ESI,‡ Table S1) are overestimates, but we deem it unlikely that this is the sole factor for two reasons: first, the MPL values back-calculated from a "reasonable" density value of $\rho = 1.5$ g cm^{-3} are far lower than even the aforementioned uncertainties can account for. The requisite mass deficit for $\rho_{SAXS,PG6} = 1.5$ g cm^{-3} for instance would amount to ~45% of the theoretically achievable mass (see ESI,‡ Table S10 and Fig. S18), a value which appears unrealistic in view of the experimentally determined mass deficiency of ~10% (see ESI,‡ Table S1). Second, these uncertainties are largely eliminated in the structurally less deficient series B.[25] Because ρ_{bulk} and ρ_{SAXS} showed the outermost extremes in values of ρ for series A, it appeared appropriate to also apply these methods to samples from series B. Qualitatively, the results for series B match those obtained for series A: for the annealed samples, it was found that $\rho_{bulk} < 1.25$ g cm^{-3}, and that ρ_{SAXS} increases with g, this time to even higher values up to $\rho_{SAXS,PG7} \approx 3.7$ g cm^{-3} (see ESI,‡ Table S8 for details). Structural deficiencies of these DPs therefore cannot be the sole cause for the extraordinarily high density values determined. This in turn suggests that systematic factors are at play, for instance an underestimate of the spacing between individual DP chains. This appears reasonable as the SAXS results for PG7 (see ESI,‡ Table S3) in part contradict the trends in chain diameters obtained from SEM/TEM, qSTEM and prior AFM results,[23] though the cause of this anomaly is currently unclear. The difference between ρ_{bulk} and ρ_{SAXS} is also much larger than one would normally expect for liquid-crystalline materials, for which the match between these values is often quite good.[38] The present DP samples are certainly partially amorphous even when annealed, as evidenced by the bulk samples being mostly translucent. However, as the DPs decompose prior to melting, we can currently not provide a good estimate of the relative proportions of self-assembled and amorphous domains within the specimen.

The electron microscopic methods – SEM/TEM and qSTEM – are also subject to further assumptions aside from MPL values: these methods provide information on the dimensions of the DPs, but the cross-section geometry of the deposited DP chains has not been determined experimentally. A cut-circular cross-section appears reasonable, particularly for the highest g polymers (see ref. 17 and ESI‡). Particularly for qSTEM, assuming different cross-section geometries may result in substantial density variation (see ESI,‡ Table S5). An additional factor of uncertainty is the possible dependence of the cross-section geometry on the substrate (mica in SEM/TEM *vs.* amorphous carbon in qSTEM). SEM/

*** For instance, the phenylalanine dimer ($C_{19}H_{22}N_2O_3{\cdot}0.5H_2O$) has a crystalline density of 1.26 g cm^{-3}; CSD No. 918326.

TEM and qSTEM measurements as described here therefore also do not provide satisfactorily reliable density values, particularly in the high g regime of prime interest.

Lastly, it should be noted that the ordered domains which are probed in SAXS likely differ from the individual-molecule samples involved in the determination of $\rho_{SEM/TEM}$ and ρ_{qSTEM}. Particularly due to differences in the packing of the outermost dendritic periphery and due to interfacial effects, it can at present not be excluded that these two types of samples have different volumetric mass densities. Though all methods suggest an increase in ρ for high g, the present data do not permit for definite conclusions in view of the uncertainties discussed above. It is however at the very least possible to more closely limit the range of possible ρ by considering ρ_{bulk}: average volume occupancies in the range of 85–100% appear possible for the bulk specimen, resulting in an estimated range of individual chain density of $\rho \approx 1.2$–1.5 g cm^{-3}. As the individual chains in the bulk state are unlikely to conform to hard cylinders (with the possible exception of $g > 6$ DPs), the chains are likely interdigitated in the annealed, bulk solids, and therefore the lower end of the estimated density range appears more realistic. Compared to the prior estimate for the possible range of DP densities of $\rho \approx 0.9$–1.5 g cm^{-3}, this new estimate constitutes an improvement insofar as it limits the possible values of the maximum dendritic generation g_{max}: for a range of $\rho \approx 1.15$–1.35 g cm^{-3}, $g_{max} = 6$, in agreement with recent experimental results concerning the swelling behaviour of DPs.[39] A value of $g_{max} < 6$ is highly unlikely, as this would require individual molecule density values $\rho < \rho_{bulk}$ (compare Fig. 1b).

Conclusions

The results presented in this publication are the test case of a particularly challenging set of samples: the investigated dendronized polymers are soft, flexible, essentially amorphous molecular objects with considerable length dispersity. Presently, the derivation of individual molecule density from SAXS, SEM/TEM or qSTEM requires external inputs and model assumptions, different for each method and at times difficult to verify experimentally. The main conclusion of the work presented here is therefore that none of the methods discussed are by themselves adequate to determine individual molecule densities in the dry state. This is further complicated by the question whether the bulk and individual molecule samples investigated may be compared at all, or whether there are differences in the real densities of these specimen.

With these uncertainties in mind, we would nevertheless like to note that all methods of density determination consistently indicate an increase of ρ for the highest g DPs, *i.e.* the true molecular objects, when compared to their low g homologs, which more closely resemble classical polymers. Though the wide spread of the present data does not permit definite conclusions, this hints at the possibility of a g-dependent increase in ρ. Not yet having comprehensive insights from molecular modelling studies, we however find it too early to speculate on possible mechanisms of self-contraction in DPs.[40]

A potential alternative method to derive individual-molecule densities presents itself thanks to recent advances in electron microscopic techniques: improvements in electron detection, microscopy instrumentation and data analysis have increased achievable signal-to-noise ratios such that, *e.g.*, the tomographic imaging of DPs in their native dissolved state has become possible.[41] In view of these advances, we propose that a combined electron microscopic method may eliminate the weaknesses of SEM/TEM and qSTEM as employed here: using state-of-the-art equipment, it should be possible to perform (cryo)-qSTEM tilt series on uncoated specimen and to analyze the data in the framework of single-particle analysis. These measurements would provide geometric information and a measure of the deposited mass from a single specimen. Alternatively, the cross-section geometry could also be explored by electron microscopy of vertical sections of the deposited DPs. The acquisition and analysis of such data will not be trivial by any means, and particular attention will have to be paid to the issues of radiation damage and thresholding, but we anticipate that the suggested approaches will provide far more accurate estimates of density – and thereby answers to the still-open questions of density trends, the comparability of bulk and individual-molecule densities, and the location of g_{max} – than are presently possible.

Author contributions

AH, ADS and MK conceived the project; DM and HY synthesized the dendronized polymers; HY and RW conducted and evaluated SEM and TEM measurements; DM conducted bulk density measurements and prepared specimen for other studies; ASF conducted and evaluated all SAXS and WAXS measurements; RW prepared initial samples for qSTEM; ST, HN and JK conducted qSTEM measurements, ST performed all qSTEM data evaluation; DM and ADS wrote the manuscript; ASF, ST, RM and MK critically reviewed the manuscript and contributed substantially to its finalization.

Conflicts of interest

There are no conflicts of interest to declare.

Acknowledgements

The authors would like to thank the staff at of ScopeM (ETH Zürich) for their help with various electron microscopic tasks. Dr Thomas Schweizer (D-MATL, ETH Zürich) is thanked for constructing the density gradient column setup, and Horst Adelmann (D-HEST, ETH Zürich) is gratefully acknowledged for help in annealing DP samples. We would also like to thank Dr Gregor Hofer and Dr Richard Whitfield (both D-MATL, ETH Zürich) for their critical reading of the manuscript.

References

1 V. Kholodovych and W. J. Welsh, Densities of Amorphous and Crystalline Polymers, in *Physical Properties of Polymers Handbook*, Springer New York, New York, NY, 2007; pp. 611–617.

2 J. Li, C. Nagamani and J. S. Moore, Polymer Mechanochemistry: From Destructive to Productive, *Acc. Chem. Res.*, 2015, **48**(8), 2181–2190.

3 S. Panyukov, E. B. Zhulina, S. S. Sheiko, G. C. Randall, J. Brock and M. Rubinstein, Tension Amplification in Molecular Brushes in Solutions and on Substrates, *J. Phys. Chem. B*, 2009, **113**, 3750–3768.

4 N. V. Lebedeva, F. C. Sun, H.-I. Lee, K. Matyjaszewski and S. S. Sheiko, ''Fatal Adsorption'' of Brushlike Macromolecules: High Sensitivity of C–C Bond Cleavage Rates to Substrate Surface Energy, *J. Am. Chem. Soc.*, 2008, **130**, 4228–4229.

5 M. Grandbois, M. Beyer, M. Rief, H. Clausen-Schaumann and H. E. Gaub, How Strong Is a Covalent Bond?, *Science*, 1999, **283**(5408), 1727–1730.

6 M. Rubinstein and R. H. Colby, *Polymer Physics*, Oxford University Press, 2003.

7 H. Frauenrath, Dendronized Polymers—Building a New Bridge from Molecules to Nanoscopic Objects, *Prog. Polym. Sci.*, 2005, **30**(3–4), 325–384.

8 A. D. Schlüter, A. Halperin, M. Kröger, D. Vlassopoulos, G. Wegner and B. Zhang, Dendronized Polymers: Molecular Objects between Conventional Linear Polymers and Colloidal Particles, *ACS Macro Lett.*, 2014, **3**(10), 991–998.

9 A. B. Cook and S. Perrier, Branched and Dendritic Polymer Architectures: Functional Nanomaterials for Therapeutic Delivery, *Adv. Funct. Mater.*, 2019, 1901001.

10 B. I. Voit and A. Lederer, Hyperbranched and Highly Branched Polymer Architectures—Synthetic Strategies and Major Characterization Aspects, *Chem. Rev.*, 2009, **109**(11), 5924–5973.

11 R. Verduzco, X. Li, S. L. Pesek and G. E. Stein, Structure, Function, Self-Assembly, and Applications of Bottlebrush Copolymers, *Chem. Soc. Rev.*, 2015, **44**(8), 2405–2420.

12 G. R. Newkome; C. N. Moorefield and F. Vögtle, *Dendrimers and Dendrons*, Wiley-VCH Verlag GmbH & Co. KGaA, Weinheim, FRG, 2001.

13 D. Yan; C. Gao and H. Frey, *Hyperbranched Polymers: Synthesis, Properties, and Applications*, Wiley, 2011.

14 Y. Zheng, S. Li, Z. Weng and C. Gao, Hyperbranched Polymers: Advances from Synthesis to Applications, *Chem. Soc. Rev.*, 2015, **44**(12), 4091–4130.

15 P. G. de Gennes and H. Hervet, Statistics of ''Starburst'' Polymers, *J. Phys., Lett.*, 1983, **44**(3), 351–360.

16 D. A. Tomalia, A. M. Naylor and W. A. Goddard III, Starburst Dendrimers: Molecular-Level Control of Size, Shape, Surface Chemistry, Topology, and Flexibility from Atoms to Macroscopic Matter, *Angew. Chem., Int. Ed. Engl.*, 1990, **29**(2), 138–175.

17 B. Zhang, R. Wepf, M. Kröger, A. Halperin and A. D. Schlüter, Height and Width of Adsorbed Dendronized Polymers: Electron and Atomic Force Microscopy of Homologous Series, *Macromolecules*, 2011, **44**(17), 6785–6792.

18 A. Kröger, B. Zhang, C. Rosenauer, A. D. Schlüter and G. Wegner, Solvent Induced Phenomena in a Dendronized Linear Polymer, *Colloid Polym. Sci.*, 2013, **291**(12), 2879–2892.

19 O. Bertran, B. Zhang, A. D. Schlüter, A. Halperin, M. Kröger, C. Alemán, D. C. Spellmeyer, T. Fox, J. W. Caldwell and P. A. Kollman, *et al.*, Computer Simulation of Dendronized Polymers: Organization and Characterization at the Atomistic Level, *RSC Adv.*, 2013, **3**(1), 126–140.

20 O. Bertran, B. Zhang, A. D. Schlüter, M. Kröger and C. Alemán, Computer Simulation of Fifth Generation Dendronized Polymers: Impact of Charge on Internal Organization, *J. Phys. Chem. B*, 2013, **117**(19), 6007–6017.

21 P. K. Maiti, T. Çağın, G. Wang and W. A. Goddard III, Structure of PAMAM Dendrimers: Generations 1 through 11, *Macromolecules*, 2004, **37**(16), 6236–6254.

22 B. Zhang, R. Wepf, K. Fischer, M. Schmidt, S. Besse, P. Lindner, B. T. King, R. Sigel, P. Schurtenberger and Y. Talmon, *et al.*, The Largest Synthetic Structure with Molecular Precision: Towards a Molecular Object, *Angew. Chem., Int. Ed.*, 2011, **50**(3), 737–740.

23 H. Yu, A. D. Schlüter and B. Zhang, Synthesis of High Generation Dendronized Polymers and Quantification of Their Structure Perfection, *Macromolecules*, 2014, **47**(13), 4127–4135.

24 H. Yu, A. D. Schlüter and B. Zhang, Synthesis of Dendronized Polymers by a ''n + 2'' Approach, *Macromolecules*, 2012, **45**(21), 8555–8560.

25 D. Messmer, M. Kröger and A. D. Schlüter, Pushing Synthesis towards the Maximum Generation Range of Dendritic Macromolecules, *Macromolecules*, 2018, **51**(14), 5420–5429.

26 L. Shu, I. Gössl, J. P. Rabe and A. D. Schlüter, Quantitative Aspects of the Dendronization of Dendronized Linear Polystyrenes, *Macromol. Chem. Phys.*, 2002, **203**, 2540–2550.

27 M. Kröger, A. D. Schlüter and A. Halperin, Branching Defects in Dendritic Molecules: Coupling Efficiency and Congestion Effects, *Macromolecules*, 2013, **46**(18), 7550–7564.

28 B. Zhang, H. Yu, A. D. Schlüter, A. Halperin and M. Kröger, Synthetic Regimes Due to Packing Constraints in Dendritic Molecules Confirmed by Labelling Experiments, *Nat. Commun.*, 2013, **4**, 1993.

29 S. Costanzo, L. F. Scherz, T. Schweizer, M. Kröger, G. Floudas, A. D. Schlüter and D. Vlassopoulos, Rheology and Packing of Dendronized Polymers, *Macromolecules*, 2016, **49**(18), 7054–7068.

30 S. Tacke, V. Krzyzanek, H. Nüsse, R. A. Wepf, J. Klingauf and R. Reichelt, A Versatile High-Vacuum Cryo-Transfer System for Cryo-Microscopy and Analytics, *Biophys. J.*, 2016, **110**(4), 758–765.

31 E. Zeitler and G. F. Bahr, A Photometric Procedure for Weight Determination of Submicroscopic Particles Quantitative Electron Microscopy, *J. Appl. Phys.*, 1962, **33**(3), 847–853.

32 D. Thomas, P. Schultz, A. C. Steven and J. S. Wall, Mass Analysis of Biological Macromolecular Complexes by STEM, *Biol. Cell.*, 1994, **80**(2), 181–192.

33 S. Müller and A. Engel, Structure and Mass Analysis by Scanning Transmission Electron Microscopy, *Micron*, 2001, **32**(1), 21–31.

34 S. A. Müller, K. N. Goldie, R. Bürki, R. Häring and A. Engel, Factors Influencing the Precision of Quantitative Scanning Transmission Electron Microscopy, *Ultramicroscopy*, 1992, **46**(1–4), 317–334.
35 A. Engel, Scanning Transmission Electron Microscopy: Biological Applications, *Adv. Imaging Electron Phys.*, 2009, **159**, 357–386.
36 R. Aebersold and M. Mann, Mass Spectrometry-Based Proteomics, *Nature*, 2003, **422**(6928), 198–207.
37 G. Zhang, R. S. Annan, S. A. Carr and T. A. Neubert, Overview of Peptide and Protein Analysis by Mass Spectrometry, *Curr. Protoc. Protein Sci.*, 2010, **62**(1), 16.1.1–16.1.30.
38 B. Mu, B. Wu, S. Pan, J. Fang and D. Chen, Hierarchical Self-Organization and Uniaxial Alignment of Well Synthesized Side-Chain Discotic Liquid Crystalline Polymers, *Macromolecules*, 2015, **47**, 2388–2398.
39 D. Messmer, O. Bertran, R. Kissner, C. Alemán and A. D. Schlüter, Main-Chain Scission of Individual Macromolecules Induced by Solvent Swelling, *Chem. Sci.*, 2019, **10**, 6125–6139.
40 J. Das, M. Yoshida, Z. M. Fresco, T.-L. Choi, J. M. J. Fréchet and A. K. Chakraborty, A Dendronized Polymer Is a Single-Molecule Glass, *J. Phys. Chem. B*, 2005, **109**, 6535–6543.
41 D. Messmer, C. Böttcher, H. Yu, A. Halperin, K. Binder, M. Kröger and A. D. Schlüter, 3D Conformations of Thick Synthetic Polymer Chains Observed by Cryogenic Electron Microscopy, *ACS Nano*, 2019, **13**, 3466–3473.

